Feedback control of instabilities in the two-dimensional Blasius boundary layer: The role of sensors and actuators

Brandt A. Belson, Onofrio Semeraro, Clarence W. Rowley, and Dan S. Henningson

Citation: Physics of Fluids **25**, 054106 (2013); doi: 10.1063/1.4804390
View online: http://dx.doi.org/10.1063/1.4804390
View Table of Contents: http://scitation.aip.org/content/aip/journal/pof2/25/5?ver=pdfcov
Published by the AIP Publishing

PHYSICS OF FLUIDS **25**, 054106 (2013)

Feedback control of instabilities in the two-dimensional Blasius boundary layer: The role of sensors and actuators

Brandt A. Belson,[1,a)] Onofrio Semeraro,[2,b)] Clarence W. Rowley,[1,c)] and Dan S. Henningson[2,d)]
[1]*Mechanical and Aerospace Engineering, Princeton University, Princeton, New Jersey 08540, USA*
[2]*Department of Mechanics, Royal Institute of Technology, KTH, Sweden*

(Received 24 October 2012; accepted 2 April 2013; published online 20 May 2013)

We analyze the effects of different types and positions of actuators and sensors on controllers' performance and robustness in the linearized 2D Blasius boundary layer. The investigation is carried out using direct numerical simulations (DNS). To facilitate controller design, we find reduced-order models from the DNS data using a system identification procedure called the Eigensystem Realization Algorithm. Due to the highly convective nature of the boundary layer and corresponding time delays, the relative position of the actuator and sensor has a strong influence on the closed-loop dynamics. We address this issue by considering two different configurations. When the sensor is upstream of the actuator, corresponding to disturbance-feedforward control, good performance is observed, as in previous work. However, feedforward control can be degraded by additional disturbances or uncertainties in the plant model, and we demonstrate this. We then examine feedback controllers in which the sensor is a short distance downstream of the actuator. Sensors farther downstream of the actuator cause inherent time delays that limit achievable performance. The performance of the resulting feedback controllers depends strongly on the form of actuation introduced, the quantities sensed, and the observability of the structures deformed by the controller's action. These aspects are addressed by varying the spatial distribution of actuator and sensor. We find an actuator-sensor pair that is well-suited for feedback control, and demonstrate that it has good performance and robustness, even in the presence of unmodeled disturbances. © *2013 AIP Publishing LLC*. [http://dx.doi.org/10.1063/1.4804390]

I. INTRODUCTION

The drag on a streamlined body increases as the surrounding flow transitions from laminar to turbulent, and delaying this transition can increase performance in many applications, such as airplanes and turbines. Many passive control techniques have been developed to delay transition, but active control, in which actuation is based on sensor measurements, has the potential to be more effective and more efficient.[6] In the present study, we focus our attention on boundary layer flows developing over a flat plate, emphasizing the influence of actuator and sensor placement on the performance and robustness of the device.

Control design for the boundary layer requires special care because the governing equations are high-dimensional and nonlinear. We begin by linearizing about the laminar convectively unstable equilibrium, since our intention is to drive the flow towards this state. Many control design techniques exist for linear systems, but they are computationally expensive to apply directly. Ideally, one

a)bbelson@princeton.edu
b)onofrio@mech.kth.se
c)cwrowley@princeton.edu
d)henning@mech.kth.se

would like to design a controller for the high-dimensional system, and then form a reduced-order approximation of this controller for actual implementation;[2] however, for fluid problems, usually computing the controller from the high-dimensional model is not computationally tractable. A common solution, and the one we adopt, is to first find a reduced-order model that approximates the original high-dimensional system, and then apply standard control design techniques on the model.

A variety of methods exist for finding reduced-order models for the purpose of control design. Perhaps the earliest such study is that of Aubry,[3] who used Proper Orthogonal Decomposition (POD) to obtain a very low-dimensional nonlinear model capturing many relevant features of the boundary layer. These POD-based approaches have been effective for some flow control problems, such as wake flows,[15] but for shear flows with large non-normality, they often require physical insight or tuning to make the models accurate and amenable to control.[16] Much of the recent work on controlling boundary layers has focused on linear models, including models based on global eigenmodes.[1,19] From a control perspective, it is most appropriate to project the governing equations onto a set of modes such that the input-output dynamics are well captured; these modes are then the most controllable and observable. A method known as the Eigensystem Realization Algorithm (ERA)[17,21,22] does approximately this, and yields a new set of states which are ranked by controllability and observability. Less controllable and observable states are easily truncated as desired, and there are *a priori* error bounds on how little the truncated model differs from the original system.

Previous studies[4,19,25] have demonstrated effective control of Tollmien-Schlichting (TS) waves in the boundary layer using active control. In Ref. 14, adaptive filters and active wave cancellation were used for feedback control of a compressible boundary layer. Other studies[4,25] used a modeling technique that is equivalent to ERA (balanced POD).[21] Our intention is to build on these previous results, and so we intentionally use a similar geometry, in order to remove unnecessary differences and ease comparison. In previous works, the sensors were placed upstream of the actuators without rigorously exploring other choices. However, the positions of the actuator and sensor can have a significant effect on the performance and robustness of the active control. For example, for the complex Ginzburg-Landau equation (a system similar to that of bluff body wakes), it was found that the optimal actuator and sensor configuration significantly increased performance.[11]

The main contribution of this work is to analyze the effect of different actuators, sensors, and their positions on the active control of the instabilities that lead to transition in the 2D spatially evolving Blasius boundary layer. This parametric analysis can be crucial when considering implementing control in experiments and applications; indeed, numerical simulations allow us to investigate the influence of many actuator and sensor positions that would be difficult and costly in physical experiments and applications, if possible at all.

We demonstrate how the relative position of the sensor and the actuator determines the controller's properties. In particular, when the sensor is located upstream of the actuator, the arrangement results in a disturbance feedforward controller, in which the effect of the downstream actuator is not detected by the upstream sensor due the convective nature of the boundary layer. This is the same setup used in previous works[4,25] and we show that the best rejection of known disturbances is achieved with this configuration. However, the performance of feedforward controllers often degrades in the presence of additional disturbances and unmodeled dynamics, while feedback controllers are usually much less sensitive to these uncertainties. For this reason, a different setup may be desirable, in which the sensor does detect the effects of the actuator, i.e., a feedback configuration with the sensor downstream of the actuator.

We shall see that the original choices of actuators and sensors are ineffective in feedback configurations. By using different actuators and sensors, however, a simple proportional-integral feedback controller performs well at rejecting disturbances and is robust to unmodeled disturbances as well. We show that the feedforward controller's performance is degraded by an additional disturbance, while the feedback controller's performance is essentially unaffected.

This article begins by explaining the physical fluids problem and defining the input forcing and output measurements in Sec. II. In Sec. III, we recast the fluid equations as a linear time-invariant system for control, and show the equivalent block diagram. We explain the control design techniques, and how we achieve an approximation of these controllers using reduced-order models. In Sec. IV,

we form the reduced-order model and observe that it accurately approximates the input-output dynamics of the original high-order system. In Sec. V, we analyze the performance of the controllers with different actuator-sensor configurations, and explain why we need to use different actuators and sensors for a feedback controller. Finally, we demonstrate that feedback control outperforms feedforward in the presence of unmodeled disturbances.

II. PHYSICAL PROBLEM

The objective of active control is to delay the transition to turbulence in the two-dimensional Blasius boundary layer by suppressing the (convectively) unstable growth of propagating disturbances. The governing equations are the incompressible Navier-Stokes equations, linearized about the zero-pressure-gradient laminar base flow, $\mathbf{V}$,

$$\frac{\partial \mathbf{v}}{\partial t} = -(\mathbf{V}\cdot\nabla)\mathbf{v} - (\mathbf{v}\cdot\nabla)\mathbf{V} - \nabla p + \frac{1}{Re}\nabla^2\mathbf{v} + \mathbf{f}$$
$$\nabla\cdot\mathbf{v} = 0. \tag{1}$$

Here, $\mathbf{v}$ is the deviation from the base flow, p is the pressure, ∇ is defined as $(\partial/\partial x,\ \partial/\partial y)$. The Reynolds number is defined as $Re = U\delta_0^*/\nu$ where U is the free-stream velocity, ν is the kinematic viscosity, and δ_0^* is the displacement thickness at the inlet of the computational domain. We use $Re = 1000$ in all cases and non-dimensionalize all lengths by δ_0^*. The incompressible linearized Navier-Stokes equations are convectively unstable at this Re, and the physical form of the instability is exponentially growing Tollmien-Schlichting (TS) waves. We consider the linearized equations because the controllers force the flow towards the laminar base flow, and so we expect the truncated nonlinear terms to be small. This approximation also allows us to use existing control, modeling, and analysis techniques available for linear systems.

A representative schematic of the problem is shown in Figure 1. Note that this arrangement is the same as in Ref. 4 for ease of comparison. The momentum equation (1) is forced with

$$\mathbf{f} = \mathbf{B}_{\mathsf{w}}(x, y)\mathsf{w}(t) + \mathbf{B}_{\mathsf{u}}(x, y)\mathsf{u}(t), \tag{2}$$

where $\mathsf{w}(t)$ is a random disturbance, sampled from a normal distribution with zero mean and unit variance, and $\mathsf{u}(t)$ is the actuator signal, provided by the controller. The terms $\mathbf{B}_{\mathsf{w}}$ and $\mathbf{B}_{\mathsf{u}}$ are the spatial distributions of the disturbance and actuator. In the case that the force is not divergence-free, then, as shown in Ref. 8, only the component of $\mathbf{f}$ that is divergence-free directly affects the velocity. The other component affects the pressure, which is not of interest in this work. The original choice of the forcing terms is drawn from previous work[4] and is

$$\mathbf{B}_{\mathsf{w}} = \mathbf{S}(35, 1), \qquad \mathbf{B}_{\mathsf{u}} = \mathbf{S}(400, 1), \qquad \text{where} \tag{3}$$

$$\mathbf{S}(x_0, y_0) = \begin{bmatrix} (y - y_0)\sigma_x/\sigma_y \\ -(x - x_0)\sigma_y/\sigma_x \end{bmatrix} \exp\left(-\left(\frac{x - x_0}{\sigma_x}\right)^2 - \left(\frac{y - y_0}{\sigma_y}\right)^2\right), \tag{4}$$

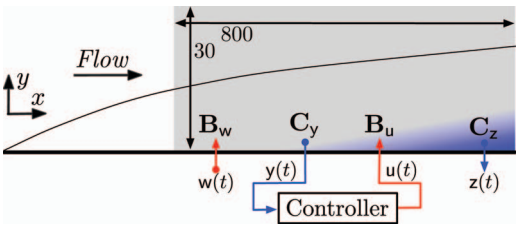

FIG. 1. Overview of boundary layer, inputs, and outputs. The grey box denotes the computational domain. The upstream disturbance is $\mathsf{w}(t)$, applied at $x_{\mathsf{w}} = 35$, and the control input is $\mathsf{u}(t)$, applied at $x_{\mathsf{u}} = 400$. The output $\mathsf{z}(t)$ is a low-order approximation of the velocity, $\mathbf{v}(t)$. Output signal $\mathsf{y}(t)$ is from a localized velocity sensor, includes noise, and its location, x_{y}, is varied.

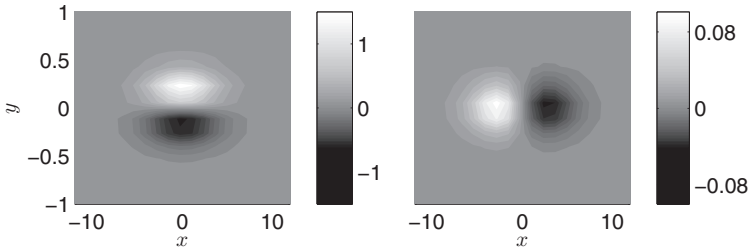

FIG. 2. Contour plots of $\mathbf{S}(0, 0)$. Left: stream-wise component. Right: wall-normal component.

where $\sigma_x = 4$ and $\sigma_y = 1/4$, shown in Figure 2. Later (Sec. V B), we choose a different form of actuation, $\mathbf{B}_\mathsf{u}$. We fix the location of the actuator at $x_0 = 400$ and vary only the sensor position because we find that, for this flow, the relative positions of the sensor and actuator are far more important than their absolute positions (also see Ref. 10).

The output spatial distributions are $\mathbf{C}_\mathsf{z}$ and $\mathbf{C}_\mathsf{y}$, and the corresponding output signals are given by

$$\mathsf{y}(t) = \int_\Omega \mathbf{C}_\mathsf{y} \cdot \mathbf{v}\, d\mathbf{x} + \mathsf{n}(t), \tag{5}$$

$$\mathsf{z}(t) = \int_\Omega \mathbf{C}_\mathsf{z} \cdot \mathbf{v}\, d\mathbf{x}, \tag{6}$$

where Ω is the computational domain. The original choice of $\mathbf{C}_\mathsf{y}$ uses the same localized spatial distribution as the actuator, $\mathbf{C}_\mathsf{y} = \mathbf{S}(x_\mathsf{u}, 1)$, where the stream-wise location of the sensor, x_0, is a key parameter investigated in Secs. IV and V. Physically, the single sensor measurement is a sum of spatial integrals of both components of velocity. The signal $\mathsf{y}(t)$ also explicitly includes noise, $\mathsf{n}(t)$, with zero mean and a variance of 0.1, a few percent of the magnitude of the noiseless signal. Our focus is not on the effect of sensor noise, hence our choice of a relatively small amount. Higher noise levels have little effect on the results presented later.

The second output signal $\mathsf{z}(t)$ is used to approximate the disturbance energy in the flow, for use in a cost function for optimal control design. The details of this method, called output projection, are explained in Sec. III B. The spatial support of $\mathbf{C}_\mathsf{z}$ is global but primarily downstream because the disturbance energy grows as it convects. While it is not realistic to construct a physical sensor to measure $\mathbf{C}_\mathsf{z}$, this does not preclude the resulting controllers from use in experiments because $\mathsf{z}(t)$ is not supplied to the controller; it is used only in the design of the controller.

III. METHODS

A. Numerical flow solver

Simulations are conducted using a pseudo-spectral solver code for incompressible boundary layer flows.[12] This solver has been extensively validated and tuned for performance,[9] and recently used in similar studies of boundary layers.[4,25] The numerical method uses Fourier modes in the stream-wise and spanwise directions, and Chebyshev modes in the wall-normal direction, and is similar to that used in Ref. 18. In order to simulate a spatially developing boundary layer, a so-called "fringe" region near the outflow boundary is implemented.[23] The domain shown in the grey box in Figure 1 excludes this non-physical fringe region, which extends another 200 δ_0^* to the right. An artificial free-stream boundary condition is enforced at the top of the domain.[5] The grid size is 784×101, and is chosen based on a resolution study for these boundary conditions and this $Re = 1000$.

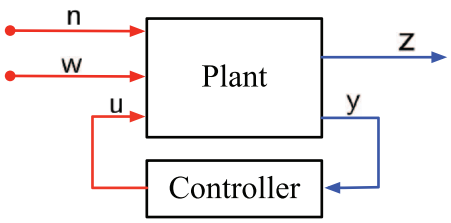

FIG. 3. Block diagram of control setup. In Figure 1, the plant is the linearized Navier-Stokes equation (7).

B. Modeling and control

In this section, we cast the flow control problem in terms of linear control theory. The discretized linearized Navier-Stokes equations (1) are expressed as a linear time-invariant system

$$\begin{aligned} \mathbf{v}_{i+1} &= \mathbf{A}\mathbf{v}_i + \mathbf{B}_\mathsf{w}\mathsf{w}_i + \mathbf{B}_\mathsf{u}\mathsf{u}_i \\ \mathsf{z}_i &= \mathbf{C}_\mathsf{z}\mathbf{v}_i \\ \mathsf{y}_i &= \mathbf{C}_\mathsf{y}\mathbf{v}_i + \mathsf{n}_i, \end{aligned} \tag{7}$$

where $\mathbf{A}$, $\mathbf{B}_\mathsf{w}$, $\mathbf{B}_\mathsf{u}$, $\mathbf{C}_\mathsf{z}$, and $\mathbf{C}_\mathsf{y}$ are linear operators, and the subscript denotes the discrete time step. As previously mentioned, only the divergence-free component of the inputs directly affects the velocity, and so the inputs in (7) are assumed to be projected onto the divergence-free space. The discrete-time formulation is used for consistency with the time-discretization of flow solvers. Note that we use the same symbols for both discrete and continuous time variables, and rely on context for distinction. We also cast the fluid system in Figure 1 as a generic plant and draw an equivalent block diagram in Figure 3.

For each position of the sensor, we design controllers to limit the growth of the disturbance energy, $\|\mathbf{v}\|^2$ with efficient use of input energy u^2. To do this on the full system is computationally expensive. Instead, we find a reduced-order model that approximates the full linearized Navier-Stokes equation and serves as the plant in Figure 3. Then we find controllers that are effective for the model, and apply these controllers to the original system.

For control design, the plant is simply a map from inputs u and w (the noise is relevant to the control, not the model) to outputs y and z as shown in Figure 3. Therefore, we seek a reduced-order model that approximates the input-output behavior of the full linearized Navier-Stokes plant; it does not necessarily need to approximate the internal state, the velocity $\mathbf{v}$. In control terminology, such a model is said to retain the most controllable and observable states and neglect the others. A state is considered highly controllable if it is easily excited by an input, and analogously, a state is considered highly observable if, when taken as an initial condition, it excites large future outputs (in the absence of inputs). A method called balanced truncation provides such a model: the state vector, $\mathbf{v}$, is linearly transformed such that each element of the state is equally controllable and observable, the state elements are ordered from most controllable/observable to least controllable/observable, and then the least controllable/observable states are truncated. While not optimal, this method provides *a priori* bounds on the difference between the original system and the model that are close to the best achievable by any model reduction method.[27] Balanced truncation is not computationally feasible directly, so we use an approximation known as the Eigensystem Realization Algorithm (ERA).[17,21,24] ERA gives theoretically equivalent reduced-order models as balanced POD,[21] which was used in previous work,[4,25] but requires no adjoint simulations and is computationally cheaper by an order of magnitude. ERA requires only a time-sampled series of outputs from an impulse-response simulation, and yields a discrete-time model.

We briefly outline the steps in computing ERA models. For a complete description, see Ref. 21. ERA requires the Markov parameters,

$$\left(\mathbf{CB},\ \mathbf{CAB},\ \mathbf{CA}^{P}\mathbf{B},\ \mathbf{CA}^{P+1}\mathbf{B},\ \ldots,\ \mathbf{CA}^{2NP}\mathbf{B},\ \mathbf{CA}^{2NP+1}\mathbf{B}\right)$$

$$\mathbf{B} \equiv \begin{bmatrix}\mathbf{B}_{\mathsf{w}} & \mathbf{B}_{\mathsf{u}}\end{bmatrix} \quad \mathbf{C} \equiv \begin{bmatrix}\mathbf{C}_{\mathsf{z}} \\ \mathbf{C}_{\mathsf{y}}\end{bmatrix},$$

which we find via simulating impulse responses in each input individually. The variable P is the number of time steps between each pair of Markov parameters, and N is the number of pairs. We arrange the Markov parameters into Hankel matrices $\mathbf{H}$ and $\mathbf{H}'$, defined by

$$H = \begin{bmatrix} \mathbf{CB} & \mathbf{CA}^{P}\mathbf{B} & \ldots & \mathbf{CA}^{NP}\mathbf{B} \\ \mathbf{CA}^{P}\mathbf{B} & \mathbf{CA}^{2P}\mathbf{B} & \ldots & \mathbf{CA}^{(N+1)P}\mathbf{B} \\ \vdots & \vdots & \ddots & \vdots \\ \mathbf{CA}^{NP}\mathbf{B} & \mathbf{CA}^{(N+1)P}\mathbf{B} & \ldots & \mathbf{CA}^{2NP}\mathbf{B} \end{bmatrix} \tag{8}$$

and

$$H' = \begin{bmatrix} \mathbf{CAB} & \mathbf{CA}^{P+1}\mathbf{B} & \ldots & \mathbf{CA}^{NP+1}\mathbf{B} \\ \mathbf{CA}^{P+1}\mathbf{B} & \mathbf{CA}^{2P+1}\mathbf{B} & \ldots & \mathbf{CA}^{(N+1)P+1}\mathbf{B} \\ \vdots & \vdots & \ddots & \vdots \\ \mathbf{CA}^{NP+1}\mathbf{B} & \mathbf{CA}^{(N+1)P+1}\mathbf{B} & \ldots & \mathbf{CA}^{2NP+1}\mathbf{B} \end{bmatrix}, \tag{9}$$

and use a singular value decomposition to write $\mathbf{H} = \mathbf{U}\boldsymbol{\Sigma}\mathbf{V}^{*}$, where $\mathbf{U}$ and $\mathbf{V}$ are unitary, $\boldsymbol{\Sigma}$ is diagonal, and $\mathbf{V}^{*}$ denotes the complex conjugate transpose of matrix $\mathbf{V}$. Then we select the order of the reduced-order model, r, and truncate the matrices, keeping the first r columns of $\mathbf{U}$ and $\mathbf{V}$ to obtain $\mathbf{U}_r$ and $\mathbf{V}_r$, and the first r rows and columns of $\boldsymbol{\Sigma}$ to obtain $\boldsymbol{\Sigma}_r$. Then we find the reduced-order model matrices,

$$\begin{aligned} \mathbf{A}_r &= \boldsymbol{\Sigma}_r^{-1/2}\mathbf{U}_r^{*}\mathbf{H}'\mathbf{V}_r\boldsymbol{\Sigma}_r^{-1/2} \\ \mathbf{B}_r &= \text{the first [number of inputs] columns of } \boldsymbol{\Sigma}_r^{1/2}\mathbf{V}_r^{*} \\ \mathbf{C}_r &= \text{the first [number of outputs] rows of } \mathbf{U}_r\boldsymbol{\Sigma}_r^{1/2}. \end{aligned} \tag{10}$$

The reduced system is

$$\begin{aligned} \mathbf{q}_{i+1} &= \mathbf{A}_r\mathbf{q}_i + \mathbf{B}_{\mathsf{w},r}\mathsf{w}_i + \mathbf{B}_{\mathsf{u},r}\mathsf{u}_i \\ \mathsf{z}_i &= \mathbf{C}_{\mathsf{z},r}\mathbf{q}_i \\ \mathsf{y}_i &= \mathbf{C}_{\mathsf{y},r}\mathbf{q}_i + \mathsf{n}_i, \end{aligned} \tag{11}$$

where $\mathbf{B}_r \equiv [\mathbf{B}_{\mathsf{w},r}\ \mathbf{B}_{\mathsf{u},r}]$ and $\mathbf{C}_r \equiv \begin{bmatrix}\mathbf{C}_{\mathsf{z},r} \\ \mathbf{C}_{\mathsf{y},r}\end{bmatrix}$. We use a slightly modified set of steps for computing many models efficiently; see the Appendix for details. The freely available `modred` library (http://pypi.python.org/pypi/modred) is used to find the ERA models.

The original state $\mathbf{v}$, and thus the disturbance energy $\|\mathbf{v}\|^2 = \langle\mathbf{v}, \mathbf{v}\rangle$, is not accessible from only the reduced-order model state $\mathbf{q}$, but is important for evaluating the effectiveness of a controller. To reproduce the full velocity would require a very large $\mathbf{C}_r$ and would defeat the purpose of the model by dramatically increasing the computational cost of control design. It is appropriate to approximate $\mathbf{v}$ by its projection onto a low-order basis with a method known as output projection.[24] This basis is spanned by the POD modes, such that $\mathbf{C}_{\mathsf{z}}$ projects the velocity onto the POD modes, i.e., $\mathsf{z} = \mathbf{C}_{\mathsf{z}}\mathbf{v}$ where z are the POD mode coefficients. The disturbance energy is optimally approximated as $\|\mathsf{z}\|_2^2$. We compute the POD modes via the method of snapshots,[26] and again make use of the freely availably `modred` library.

The models are used for two different types of control design: H_2-optimal control and proportional-integral (PI) feedback (see a standard textbook).[27] Many other types of control design exist, but these are selected because they are common, have clear physical meanings, and are the simplest that demonstrate our results. To facilitate both types of control design, we return to continuous time and write the plant transfer function, $\mathbf{P}(s)$, as

$$\begin{bmatrix} \mathsf{z}' \\ \mathsf{y} \end{bmatrix} = \mathbf{P}(s) \begin{bmatrix} \mathsf{w} \\ \mathsf{n} \\ \mathsf{u} \end{bmatrix} = \begin{bmatrix} \mathbf{P}_{\mathsf{w},\mathsf{z}'}(s) & \mathbf{P}_{\mathsf{n},\mathsf{z}'}(s) & \mathbf{P}_{\mathsf{u},\mathsf{z}'}(s) \\ P_{\mathsf{w},\mathsf{y}}(s) & P_{\mathsf{n},\mathsf{y}}(s) & P_{\mathsf{u},\mathsf{y}}(s) \end{bmatrix} \begin{bmatrix} \mathsf{w} \\ \mathsf{n} \\ \mathsf{u} \end{bmatrix}, \tag{12}$$

where $\mathsf{z}' = [\mathsf{z} \quad \mathsf{u}]^T$ is used as the objective to keep small, and s is the complex frequency (the Laplace transform of time). The noise is only in the sensor, so $\mathbf{P}_{\mathsf{n},\mathsf{z}'}(s) = 0$ and $P_{\mathsf{n},\mathsf{y}}(s) = 1$. We do not place weights on z or u as our focus is primarily on the feasibility of feedback control, not specific performance goals. The controller transfer function is $K_{\mathsf{y},\mathsf{u}}$, $\mathsf{u} = K_{\mathsf{y},\mathsf{u}}\mathsf{y}$. The closed-loop transfer function from exogenous inputs w and n to objective z' is given by the linear fractional transform

$$F_l(\mathbf{P}, K_{\mathsf{y},\mathsf{u}}) = \mathbf{P}_{\mathsf{wn},\mathsf{z}'} + \mathbf{P}_{\mathsf{u},\mathsf{z}'} K_{\mathsf{y},\mathsf{u}} (1 - P_{\mathsf{u},\mathsf{y}} K_{\mathsf{y},\mathsf{u}})^{-1} P_{\mathsf{wn},\mathsf{y}}. \tag{13}$$

The first type of control, H_2-optimal, finds the controller, $K_{\mathsf{y},\mathsf{u}}$, that minimizes cost

$$\text{cost} = \|F_l(\mathbf{P}, K_{\mathsf{y},\mathsf{u}})\|_2^2 = E(\|\mathsf{z}'\|_2^2)/E(\mathsf{w}^2 + \mathsf{n}^2), \tag{14}$$

where $E(\cdot)$ denotes the expected value. Physically, this is the optimal tradeoff between minimizing the disturbance energy and actuation energy. For more details, see a standard textbook.[27]

The second type of control, PI, determines the input signal, u, based on the sum of the sensor measurement and its integral: $\mathsf{u}_i = k_P \mathsf{y}_i + k_I \sum_{j=1}^{i} \mathsf{y}_j$, where k_P and k_I are the proportional and integral gains. The proportional term simply forces the flow proportionally to the difference in y from undisturbed laminar flow. The integral term improves the effectiveness by adding the sum of all previous differences in y from undisturbed laminar flow. The two gains are tuned, and will be chosen to effectively reduce $E(\|\mathsf{z}'\|_2^2)$.

IV. MODEL REDUCTION RESULTS

The first ten POD modes capture over 90% of the disturbance energy and define $\mathbf{C}_{\mathsf{z}}$. Figure 4 shows the first four. The spatial support is concentrated downstream, where the energy has been amplified by the flow. The modes appear in pairs because of the traveling structure of the TS waves. Since the modes are real (no imaginary part), a pair is required to span the different phases.

We find that the ERA reduced-order models are accurate with $r = 70$ states. This is supported by the 70th singular value being several orders of magnitude smaller than the first (Figure 5), and by the small amount of error between the model and direct numerical simulations (DNS) impulse

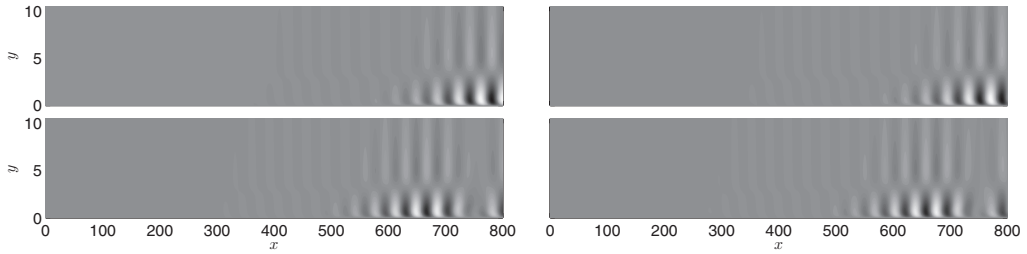

FIG. 4. Contour plots of stream-wise velocity of the leading POD modes. Dark corresponds to negative and light to positive, ranging from −0.08 to 0.08.

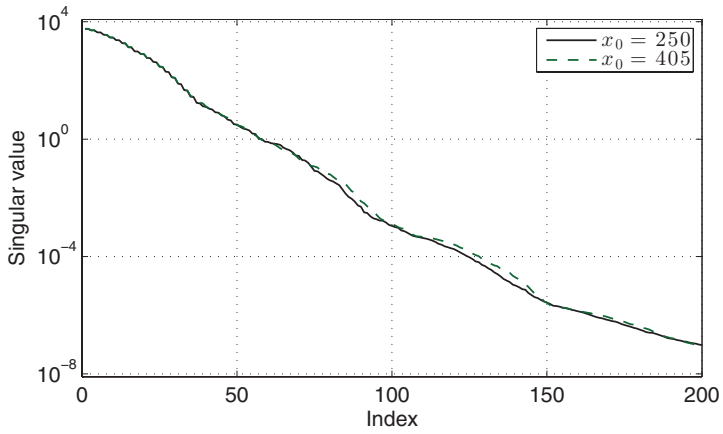

FIG. 5. Singular values of the Hankel matrices for $\mathbf{C}_\mathsf{y}$ centered at $x_\mathsf{y} = 250$ and $x_\mathsf{y} = 405$.

responses shown in Figure 6. More states are required than in previous studies[16] due to the large time delays present in this system. The delays exist because the spatially localized inputs in w and u generate perturbations that must convect significantly downstream before the output signals are non-zero. Approximations (such as Padè approximations) of time delays typically need to be high order if the delay is large, as is the case here.

In Figure 6, showing input u to output y, the signal is essentially zero because the sensor, $\mathbf{C}_\mathsf{y}$, is upstream of the actuator, $\mathbf{B}_\mathsf{u}$. This highlights an important difference between two classes of actuator-sensor configurations; if the sensor measures the effect of the actuator, then this is a feedback configuration since the controller has information about its effectiveness fed back to it. The flow is highly convective, so this can only occur when the sensor is very near or downstream of the actuator. Conversely, if the sensor does not sense the effect of actuator, then this is a feedforward control configuration. Even though the flow is incompressible and all effects are technically global, we observe that the effect of the actuator is negligible at points significantly upstream of the actuator. This distinction is explained mathematically in Ref. 28, where, within the output feedback control framework, this special case is referred to as disturbance feedforward controller, because only the disturbance is sensed.

The two categories of control types are depicted as block diagrams in Figure 7, which are equivalent to the first (Figure 3), but broken into four components. The feedback loop in Figure 7(a) between u and y does not exist in the disturbance feedforward case. In previous works[4,25] the sensor

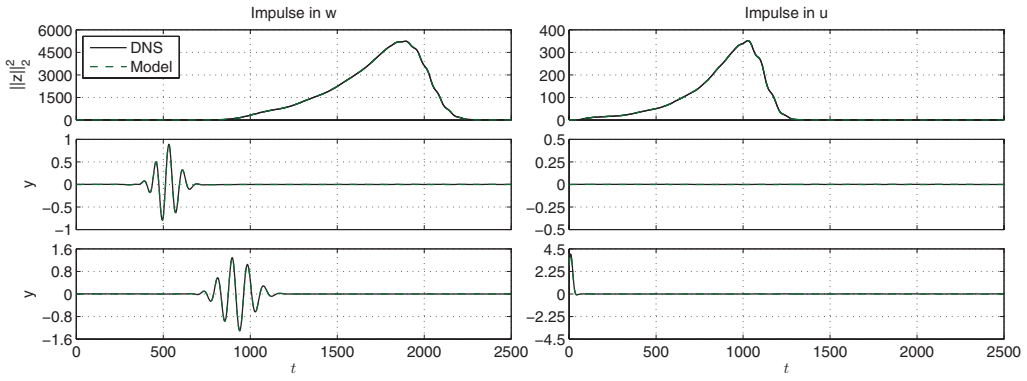

FIG. 6. Comparison of impulse responses in both inputs to both outputs. Two sensor positions are shown. The second row has $\mathbf{C}_\mathsf{y}$ centered at $x_\mathsf{y} = 250$ and the third row has $\mathbf{C}_\mathsf{y}$ centered at $x_\mathsf{y} = 405$. The maximum difference between the full system (DNS) and model among all plots is 9.1×10^{-3}.

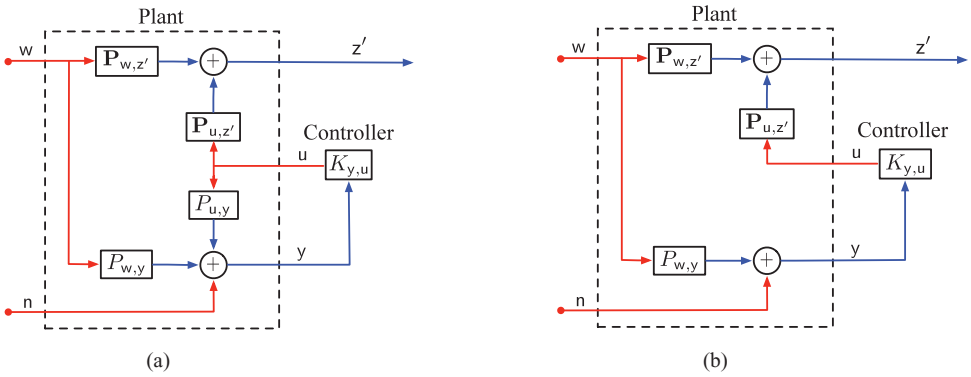

FIG. 7. Comparison of feedback and feedforward actuator-sensor configurations. (a) Feedback, $P_{u,y} \neq 0$. (b) Feedforward, $P_{u,y} = 0$. The dashed box denotes the plant, similarly to Figure 3.

is upstream of the actuator (centered at $x_y = 300$), resulting in a disturbance feedforward control configuration.

The difference between feedforward and feedback control is more than semantics—the two types of control have fundamentally different properties. For many systems, feedback controllers offer advantages over feedforward controllers, such as increased effectiveness in the presence of plant uncertainties and unknown disturbances. In Sec. V, we examine the effects of sensor position and feedforward versus feedback control.

V. CHOICE OF ACTUATOR, SENSOR, AND THEIR POSITIONS

A. Original actuators and sensors

We begin by varying the position (x_y) of the sensor $\mathbf{C}_y$. For each sensor position, the positions of $\mathbf{B}_w$, $\mathbf{B}_u$, and $\mathbf{C}_z$ are unchanged, and we form a new ERA model from existing snapshots (see Appendix). We compute a H_2-optimal controller for each model and apply it to the full linearized Navier-Stokes system. The resulting performance of the controllers as a function of sensor position is shown in Figure 8.

First, we focus on the sensor positions in feedforward arrangements where $\mathbf{C}_y$ is centered at $x_0 < 390$. Figure 8(a) shows that these sensor locations result in controllers that reduce the cost (Eq. (14)) to less than 2% of the uncontrolled cost when applied to both the model and the full system (DNS). It is clear that any sensor position upstream of the actuator results in the same good performance. Physically, feedforward is effective because the TS waves retain their structure as they amplify and convect from the sensor to the actuator. This is effectively approximated by the H_2-optimal controller and the TS waves are damped by the controller as they convect by the actuator.

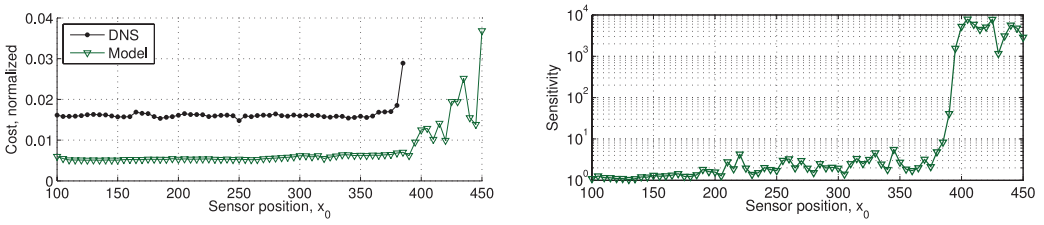

FIG. 8. (a) Cost of H_2-optimal controlled simulations normalized by the uncontrolled cost, $\|F_l(\mathbf{P}, K_{y,u})\|_2^2 / \|\mathbf{P}_{wn,z'}\|_2^2$. (b) Infinity norm of sensitivity function, $\|S\|_\infty$, for H_2-optimal controllers. In both figures, the actuator is centered at $x_0 = 400$. The controlled full system is unstable for $\mathbf{C}_y$ centered at $x_0 \geq 390$.

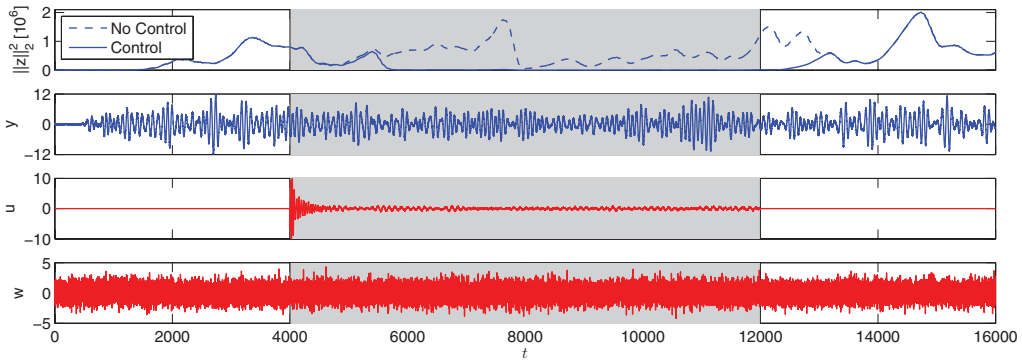

FIG. 9. Input and output signals of H_2-optimal controlled full system with sensor $\mathbf{C}_\mathsf{y}$ centered at $x_\mathsf{y} = 250$ (feedforward). The control is on from $t = 4000$ to 12000, the grey region.

The feedforward-controlled full system is excited by a stochastic disturbance and sensor noise, and the input and output signals are shown in Figure 9. This case has the sensor centered at $x_\mathsf{y} = 250$, and is representative of all feedforward configurations. The controller effectively drives the approximate energy towards zero and uses relatively low levels of control, u, so the cost (Eq. (14)) is low. The time delay of about 2000 time units between when control is turned on and when the disturbance energy begins decreasing is due to the convective nature of the boundary layer. The time delay is 2000 time units because the domain is long ($800\delta_0^*$), and the convection speed in this near-wall region is less than one. The same time delay is observed when the existing disturbed flow downstream of the sensor exits the domain. There is no need to try other actuators, sensors, or control design techniques for feedforward control because this choice is very effective and it has been explored before.[4,19]

Figure 8 also shows that the controller is more effective when applied to the model than the full system, and this is because the controller was computed specifically for the model. The slight difference between the input-output behavior of the full system and model results in slightly degraded performance. Since this is feedforward control, the stability is unaffected by this small error in approximating the plant.

However, when the sensor is further downstream and in the feedback regime, i.e., where the effect of $\mathbf{B}_\mathsf{u}$ is sensed by $\mathbf{C}_\mathsf{y}$ for $x_\mathsf{y} \geq 390$, this small difference results in instability for the full controlled system. Thus, the full system's controlled cost is infinite and omitted from Figure 8. The instability is due to a lack of robustness, and is an issue only for feedback controllers in which the stability can be changed by the controller. Robustness can be quantified as the infinity norm of the sensitivity transfer function $S(s)$,

$$S(s) = \frac{1}{1 - P_{\mathsf{u},\mathsf{y}}(s)K_{\mathsf{y},\mathsf{u}}(s)}, \tag{15}$$

where, for good stability margins, one generally seeks $\|S\|_\infty$ to be less than 2.0.[27] Figure 8 shows $\|S\|_\infty$ versus sensor location. For upstream sensors, robustness is a non-issue ($P_{\mathsf{u},\mathsf{y}}(s) \approx 0$ and deviations from $S(s) \approx 1$ are negligible). When feedback from u to y exists and $P_{\mathsf{u},\mathsf{y}}$ becomes significantly non-zero, $\|S\|_\infty$ is much greater than 2.0 and even small errors between the model and the full system result in instability.

Physically, the actuation influences the flow field and sensor slightly out of phase with how it is modeled. A measure of robustness related to $\|S\|_\infty$ is the phase margin, the amount of allowable phase error before instability. Typically, it is designed to be a minimum of 45° but for these feedback controllers it is very low—less than 0.01°. Therefore, when the effect of the actuation is fed back to the controller, it actuates with a phase that adds to the disturbance, and instability results. Sensor noise tends to expedite this process, but instability is present in the absence of noise. The same low

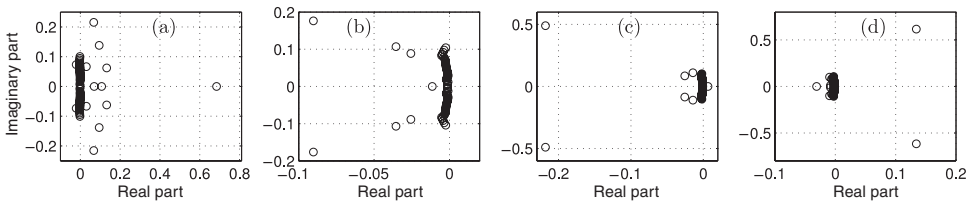

FIG. 10. Zeros of transfer function $P_{\mathsf{u},\mathsf{y}}$ for four cases: (a) original actuator and sensor at $x_{\mathsf{y}} = 450$ with minimum RHP zeros at $s = 0.03 \pm 0.067i$; (b) original actuator and sensor at $x_{\mathsf{y}} = 405$ with no RHP zeros; (c) original actuator and point sensor at $x_{\mathsf{y}} = 405$ with minimum RHP zero at $s = 0.0065$; and (d) new actuator and point sensor at $x_{\mathsf{y}} = 405$ with minimum RHP zeros at $s = 0.13 \pm 0.62i$.

levels of phase error exist in feedforward controllers, but because the error is not fed back, control is not destabilizing.

Generally, poor robustness has a variety of root causes. To identify the root causes here, we divide the feedback configurations into two cases: when the sensor is far downstream of the actuator (roughly $x_{\mathsf{y}} > 415$) and when the sensor is closer to the actuator (roughly $390 \leq x_{\mathsf{y}} \leq 415$). In the first case, the sensor measures the effect of the actuator on the flow after a significant time delay due to the highly convective nature of the boundary layer at this Re. This results in right-half plane (RHP) zeros in the transfer function from actuator to sensor, $P_{\mathsf{u},\mathsf{y}}$. RHP zeros are problematic in control design because, following the "weighted sensitivity integral,"[27] the frequency at which they exist is the approximate maximum bandwidth, or the maximum frequency that can be controlled with good performance and robustness. Therefore, RHP zeros at low frequencies place severe restrictions on the tradeoff between performance and robustness. Figure 10 shows that for the sensor at $x_0 = 450$, the most restrictive (minimum) RHP zero is at $s = 0.03 \pm 0.067i$, or a frequency of $|s| = 0.073$. In Ref. 4, it is shown that the disturbance is amplified at frequencies up to approximately $|s| = 0.12$, thus requiring a bandwidth of at least 0.12, significantly higher than 0.073. Thus, it is impossible to find controllers with good performance and robustness for this actuator-sensor pair.

A physical interpretation is the sensor measures flow structures that convected past the actuator at a previous time. The flow structures convecting over the actuator at any time cannot be approximated well by the sensor's outdated information. Thus the control signal cannot be chosen so as to cancel the flow structures convecting over the actuator. This time delay is present for any choice of localized actuator and sensor. Therefore, no controller can perform well and have good robustness, and we restrict our focus to the second case: feedback configurations with the sensor near the actuator.

Specifically, we focus on a feedback configuration with the sensor centered at $x_{\mathsf{y}} = 405$. In this case, as we show over the remainder of this section and Sec. V B, the cause of the controller's lack of robustness is not a time delay but a property of this actuator-sensor pair. We begin by noting that H_2-optimal controllers have no guaranteed stability margins[13] and in practice tend to lack robustness. A natural first thought, then, is that while H_2-optimal controllers are not robust, other controllers using this actuator-sensor pair may be robust and perform well. This notion is not supported by the controllers we try. First, methods to recover robustness from a H_2-optimal controller, such as loop-transfer recovery, are not effective here because there are zeros near the imaginary axis (Figure 10), which can result in highly oscillatory dynamics and ineffective control.[27]

In an effort to achieve better robustness, we consider tuning simple PI controllers. The frequency response of $P_{\mathsf{u},\mathsf{y}}$ is shown in the Bode plot in Figure 11. Since TS wave disturbances exist at low frequencies, we want the controller to respond aggressively to low frequency signals. Thus the loop transfer function ($P_{\mathsf{u},\mathsf{y}} K_{\mathsf{y},\mathsf{u}}$) should have a high magnitude (gain) at low frequencies. A simple proportional controller ($k_P = 1$ and $k_I = 0$) achieves this, since $P_{\mathsf{u},\mathsf{y}}$ is already large at low frequencies. With such a controller, the bandwidth (frequency at which the magnitude is 0 dB) is greater than the required 0.12 and the phase margin (phase at the same frequency) is greater than 45°. We find that this controller is robust but does not significantly reduce the disturbance energy as compared to the uncontrolled case, $\|F_l(\mathbf{P}, K_{\mathsf{y},\mathsf{u}})\|_2^2 / \|\mathbf{P}_{\mathsf{wn},\mathsf{z}'}\|_2^2 \approx 0.9$. The controller effectively forces y to be nearly

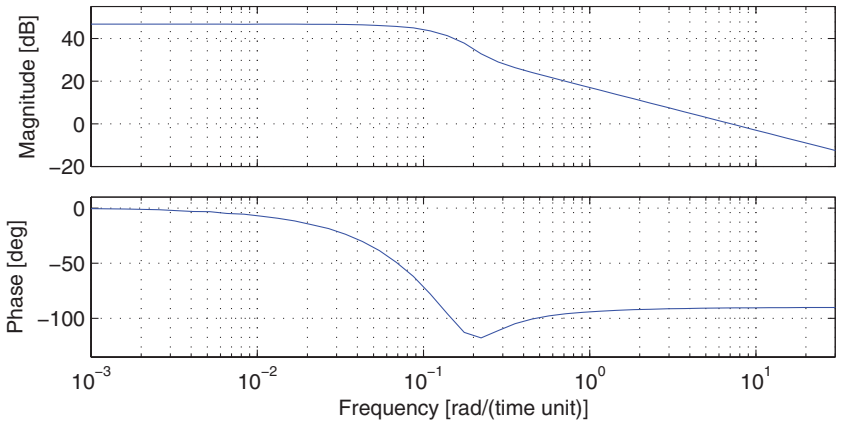

FIG. 11. Frequency response (Bode plot) of $P_{u,y}$ with original actuator and sensor centered at $x_0 = 405$.

zero, but the disturbance energy is relatively unaffected, shown in Figure 12. For other choices of gains k_P and k_I, the results are nearly unchanged; the sensor signal is forced to zero and the energy is relatively unaffected. Forcing the sensor measurement to zero would be desirable if the measurement was correlated with the structures one wants to diminish, as it often is. However, in this case the actuation only deforms the TS waves to be a slightly different fluid structure—a structure that is poorly observed by these sensors. The controller effectively cancels only the observable component of the deformed TS wave structure, but that component contains little disturbance energy. Put another way, the deformed TS waves are strongly controllable by the disturbance input, but weakly observable by the sensor.

The poor observability of the deformed TS waves (after actuation) is attributed to this sensor, which measures a linear combination of localized stream-wise and wall-normal velocities (Figure 2). Figure 13 shows the effect of the actuation on the stream-wise velocity. The plot on the left shows the uncontrolled TS wave, and the plot on the right shows the deformed TS wave has two peaks of roughly equal magnitude. These peaks align with those in the stream-wise component of the sensor's spatial distribution (Figure 2), resulting in a nearly zero sensor measurement (Eq. (6)). Only this linear combination of velocities is nearly zero, and the deformed TS waves are not significantly damped, continuing to grow downstream.

In Sec. V B, we show that different actuator-sensor pairs have different properties that make feedback control effective. Thus the reason we do not find a feedback controller for this sensor-actuator pair with good performance and robustness is attributable to this pair and the poor observability of the deformed TS waves.

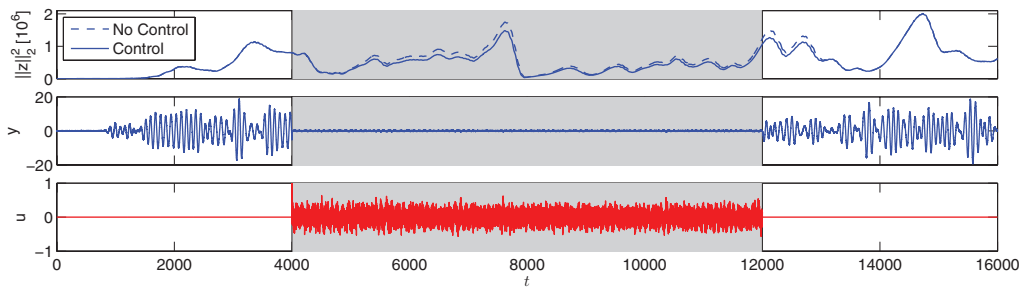

FIG. 12. Input and output signals of proportional feedback control of the full system with the original actuator and original sensor centered at $x_y = 405$ (feedback). The control is on from $t = 4000$ to 12 000 in the grey region. The disturbance signal, w, is the same as in Figure 9.

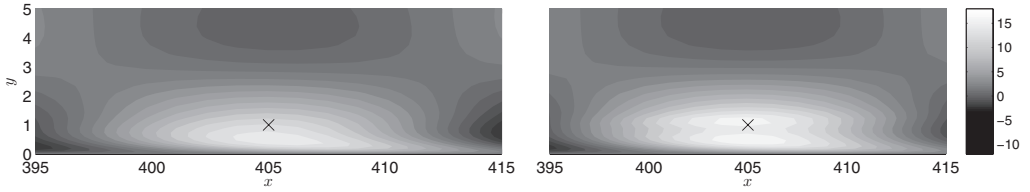

FIG. 13. Contour plots of instantaneous stream-wise velocity around sensor location $x_y = 405$, denoted by a cross. Left: Uncontrolled. Right: Proportionally controlled with original actuator-sensor pair, at time $t = 4876$. Even though the sensor measurement is nearly zero (Figure 12), the overall velocity field shows little change.

B. New actuators and sensors for feedback

The previous actuator-sensor pair resulted in poor feedback controllers since the TS waves, deformed by actuation, were poorly observable. By choosing new actuators and sensors, we overcome this and design an effective feedback controller.

We begin by simplifying the sensor from the spatial distribution given in (3) to a point sensor so that $\mathbf{C}_y$ measures only the stream-wise, dominant, component of velocity at $x_y = 405$ and $y_y = 1$. We choose this sensor because it simplifies the input-output dynamics for easier interpretation and controller design. It measures the TS wave structure more directly than the original sensor does. Further, it is only a slight modification of the original sensor, and it allows us to achieve our primary goal of comparing feedforward and feedback control. Larger changes to the sensor (or actuator) could potentially give even better performance, robustness, or increased ease of practical implementation, but optimizing the sensor is not our primary goal here.

At first we do not change the actuators from those previously described. The new ERA model is as accurate as those for the original sensors. We find though that the resulting model has a transfer function from input u to output y with a real right-half-plane zero at frequency $s = 0.0065$ (see Figure 10), which again is less than the required minimum bandwidth of 0.12. Thus, it is impossible to find a feedback controller with good performance and robustness for this actuator-sensor pair.

We chose a different actuator that directly and immediately affects the TS waves, and does not result in a plant with RHP zeros at low frequencies (disturbance input, $\mathbf{B}_w$, is unchanged). We use a Gaussian distribution that forces only in the stream-wise direction, since this is the dominant direction of the flow, and the stream-wise disturbance velocity is significantly larger than the wall-normal component,

$$\mathbf{B}_u = \left(\exp\left(-\left(\frac{x - x_0}{\sigma_x}\right)^2 - \left(\frac{y - y_0}{\sigma_y}\right)^2\right),\ \ 0\right). \tag{16}$$

By directly opposing the growth of the unstable TS waves, we expect this actuator to have the simple and predictable effect of reducing the magnitude of the TS waves. In contrast, more complicated actuators can create more complicated actuator-flow interactions, which can result in undesirable behavior (such as RHP zeros) in the input-output system, as seen with the previous choice of actuator. Figure 10 shows that there are RHP zeros at $s = 0.13 \pm 0.62i$, but $|s| = 0.63$ is greater than the required bandwidth, 0.12, and so the RHP zeros are not problematic. ERA models with $r = 70$ states are again accurate. Generally, the choice of actuator and sensor requires physical insight. A rigorous and general study would be valuable, but is not our intention. Instead, we use knowledge about the flow to find a simple choice that is effective for feedback control (as will be shown), and generally advocate this type of approach. Other choices of actuator and sensor can be effective; for example, wall-normal actuation has been used in related studies.[7,20]

The H_2-optimal feedback controllers using this actuator-sensor pair suffers the same drawbacks as the original pair—high performance but with unacceptably poor robustness. Again, lack of robustness is a common drawback of H_2-optimal controllers and methods to recover robustness are not applicable due to many zeros near the imaginary axis and in the RHP.[27]

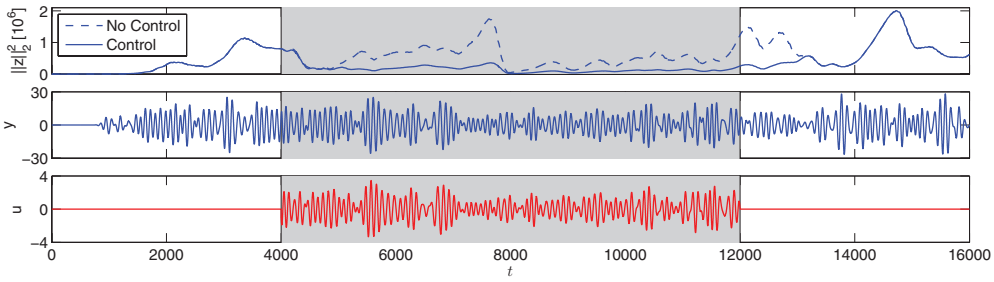

FIG. 14. Input and output signals of PI feedback controlled full system with the new actuator, Eq. (16), and a stream-wise velocity point sensor centered at $x_y = 405$ (feedback). The control is on from $t = 4000$ to 12000, the grey region. The disturbance signal, w, is the same as in Figure 9.

However, PI control has good performance and robustness. We begin by choosing gains k_P and k_I that give an acceptable phase margin and high magnitude loop gain at low frequencies. Tuning the gains results in a robust controller with $\|S\|_\infty = 1.5$, less than the maximum guideline value of 2.0, and a phase margin of 70°, above the minimum guideline value of 45°. Due to improved robustness, the control is not destabilizing when applied to the original full system. The approximate disturbance energy, $\|z\|_2^2$, versus time is shown for the full system in Figure 14, and the overall cost (Eq. (14)) is less than 25% of the uncontrolled case. While the performance is not as good as feedforward's, which reduces the cost to about 2% of the uncontrolled case, it is an effective controller. More interestingly, it is robust to plant perturbations and unknown disturbances. More advanced robust control design techniques might further improve the performance of feedback control.

C. An unmodeled disturbance's effect

To concretely demonstrate an instance where feedback is preferable to feedforward, we include a second random disturbance that is unaccounted for in the control design. Generally speaking, any disturbance downstream of the actuator is impossible to damp since the flow structures cannot be sensed and then influenced by the actuator because the flow is highly convective. However, it is possible, and desirable, for any disturbance upstream of the actuator to be damped by the controller.

We place an additional, unmodeled, disturbance at $x = 300$ (defined by $\mathbf{S}(300, 1)$) and the corresponding disturbance signal has a variance of 5.0. This is downstream of the feedforward sensor at $x_y = 250$. Thus the new disturbance's effect is not sensed and the feedforward controller is ineffective, only reducing the cost to 82% of the uncontrolled cost. The time signals are shown in Figure 15. One could, of course, place the feedforward sensor downstream of the new disturbance, for example, at $x = 350$, but this is missing the issue. The location of the unmodeled disturbance is unknown during the control design, and, as mentioned before, we desire a controller that damps any disturbance upstream of the actuator.

A feedback controller, with a sensor downstream of the actuator, can damp any unmodeled disturbance upstream of the actuator. In our example, we find that the feedback controller reduced

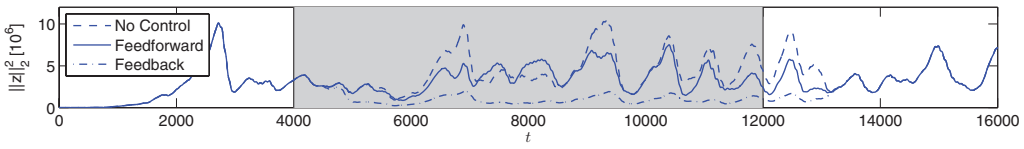

FIG. 15. Shown is a comparison of the effectiveness of feedforward and feedback controllers when a second, unmodeled, disturbance is introduced at $x = 300$. The feedforward controller uses the original actuator and sensor, and the sensor is given by $\mathbf{S}(250, 1)$. The feedback controller uses the new actuator and point sensor at $x_y = 405$.

the cost to 20% of the uncontrolled case. This is much better than the 82% achieved by the feedforward controller, and also similar to the case with only the modeled disturbance (25%). Overall we find that larger unmodeled disturbances worsen the feedforward controller's performance, but have almost no effect on the feedback controller's performance.

VI. CONCLUSIONS

We use the Eigensystem Realization Algorithm to model the 2D linearized Blasius boundary layer flow, then design controllers for the reduced-order models and apply them to the original high-order system. We investigate the role of placement and choice of the actuator and sensor on performance, stability, and robustness of the closed-loop. Due to the highly convective nature of the system, an upstream sensor cannot significantly sense the effect of the downstream actuator, even though this is incompressible flow. Thus the relative positions of the sensor and actuator dictate whether control is feedforward or feedback. We confirm the physical intuition that a feedforward configuration performs best, and that the particular upstream location is relatively unimportant.

However, feedforward controllers have many significant drawbacks. Their performance depends on the accuracy of the model, and so they are ineffective in the presence of unmodeled disturbances and perturbations. Therefore, feedback configurations are attempted. Our first finding is that the original choice of actuator and sensor was poor for feedback, both with H_2-optimal and PI controllers. The Tollmien-Schlichting waves are deformed by the actuation in such a way that they were poorly observable due to the choice of sensor, which outputs a localized linear combination of velocity components. The H_2-optimal controllers perform well on the model, but are not robust. The PI controllers are robust and significantly reduce the sensor signal, y, but perform poorly at reducing the disturbance energy. For feedback, this strict tradeoff between performance and robustness renders this actuator-sensor pair ineffective.

We change the sensor to be a simple point sensor of the stream-wise velocity. This actuator-sensor pair results in a transfer function from actuator to sensor, $P_{\mathsf{u,y}}$, which has a RHP zero at low frequency. This places severe limitations on performance and robustness, preventing any controller from being developed.

We then change the actuator to be a Gaussian distributed force in the stream-wise direction so $P_{\mathsf{u,y}}$ has no RHP zeros. The H_2-optimal controllers are again not robust. However, the PI controller performs well and is robust, reducing the objective cost to about 25% of the uncontrolled cost. Thus feedback control is shown to be effective for the boundary layer.

Feedback configurations where the sensor is far downstream of the actuator have large time delays which also cause RHP zeros in the transfer function $P_{\mathsf{u,y}}$, and this severely limits the tradeoff between performance and robustness. Thus, for any localized actuator and sensor, feedback control can be effective only when the sensor is near the actuator.

We demonstrate that feedback control outperforms feedforward control in the presence of unmodeled disturbances. A second disturbance is introduced downstream of the feedforward sensor. The feedforward controller reduces the cost to only 82% of the uncontrolled case, while the feedback controller reduces the cost to 20% of the uncontrolled case. Thus for cases where the unmodeled disturbances are known to be small, feedforward control is a good choice; otherwise, feedback control is the better choice. This flow is only convectively unstable (not absolutely unstable), and so the linear system (7) is stable, and feedforward control alone can potentially perform well. However, for absolutely unstable flows, such as the wake behind a bluff body, the linear system has unstable poles, and feedback control is necessary, since feedforward control cannot change the pole locations.

A similar analysis for the case of 3D bypass transition and the corresponding stream-wise streak structures would be interesting. In contrast to TS waves, stream-wise streaks do not strongly vary in the stream-wise direction, the direction of information flow. Thus, good performance and robustness might be obtained without requiring as careful consideration of actuators and sensors.

ACKNOWLEDGMENTS

This work was supported by the National Science Foundation, award CMMI-0932928.

APPENDIX: EFFICIENT CALCULATION OF MANY ERA MODELS

We make two slight modifications to the procedure from Sec. III B for increased accuracy and computational efficiency. The first accounts for the different amplitudes of the output signals. The magnitude of output y is much smaller than that of z, and so ERA tends to weight the observability space in favor of z, resulting in the truncation of states that improve the accuracy of y, but y is vital for the controller. To remedy this, we normalize all of the outputs before applying ERA, then adjust the resulting model. Specifically, we collect the Markov parameters, then divide all y_i by their maximum, $\mathsf{y}_{\max}$ and all z_i by the single maximum of all ten signals, $z_{\max}$. We then perform the rest of the ERA procedure, which provides the reduced-order model matrices specified in Eq. (11). Then $\mathbf{C}_{\mathsf{y},r} \mapsto \mathbf{C}_{\mathsf{y},r} \cdot \mathsf{y}_{\max}$ and $\mathbf{C}_{\mathsf{z},r} \mapsto \mathbf{C}_{\mathsf{z},r} \cdot z_{\max}$.

The second modification increases the computational efficiency of calculating of many ERA reduced-order models. Each model depends on $\mathbf{B}$ and $\mathbf{C}$, so each sensor location requires a new model. However, in this work the inputs are mostly kept fixed and the position of the outputs is varied, i.e., we primarily change $\mathbf{C}_{\mathsf{y}}$. Instead of simulating an impulse response and collecting the series of Markov parameters $\mathbf{C}\mathbf{A}^i\mathbf{B}$ for each choice of $\mathbf{C}_{\mathsf{y}}$, we collect the full snapshots $\mathbf{A}^i\mathbf{B}$. Then, for each choice of $\mathbf{C}_{\mathsf{y}}$, we compute $\mathbf{C}\mathbf{A}^i\mathbf{B}$ as post-processing. This means we do only two impulse responses for each $\mathbf{B}$ (one per input) rather than two impulses per sensor location. The same series of snapshots, $\mathbf{A}^i\mathbf{B}$, is also used when finding the POD modes.

[1] E. Åkervik, J. Hœpffner, U. Ehrenstein, and D. S. Henningson, "Optimal growth, model reduction and control in a separated boundary-layer flow using global eigenmodes," J. Fluid Mech. **579**, 305–314 (2007).
[2] B. D. O. Anderson and Y. Liu, "Controller reduction: concepts and approaches," IEEE Trans. Autom. Control **34**(8), 802–812 (1989).
[3] N. Aubry, P. Holmes, J. L. Lumley, and E. Stone, "The dynamics of coherent structures in the wall region of a turbulent boundary layer," J. Fluid Mech. **192**, 115–173 (1988).
[4] S. Bagheri, L. Brandt, and D. S. Henningson, "Input-output analysis, model reduction and control of the flat-plate boundary layer," J. Fluid Mech. **620**, 263–298 (2009).
[5] F. P. Bertolotti, T. Herbert, and P. R. Spalart, "Linear and nonlinear stability of the Blasius boundary layer," J. Fluid Mech. **242**, 441–474 (1992).
[6] T. R. Bewley and J. Kim, "A linear systems approach to flow control," Annu. Rev. Fluid Mech. **39**, 383–417 (2007).
[7] T. R. Bewley and S. Liu, "Optimal and robust control and estimation of linear paths to transition," J. Fluid Mech. **365**, 305–349 (1998).
[8] T. R. Bewley, R. Temam, and M. Ziane, "A general framework for robust control in fluid mechanics," Physica D **138**, 360–392 (2000).
[9] L. Brandt, P. Schlatter, and D. S. Henningson, "Transition in boundary layers subject to free-stream turbulence," J. Fluid Mech. **517**, 167–198 (2004).
[10] L. Brandt, D. Sipp, J. O. Pralits, and O. Marquet, "Effect of base-flow variation in noise amplifiers: the flat-plate boundary layer," J. Fluid Mech. **687**, 503–528 (2011).
[11] K. K. Chen and C. W. Rowley, "H2 optimal actuator and sensor placement in the linearised complex Ginzburg-Landau system," J. Fluid Mech. **681**, 241–260 (2011).
[12] M. Chevalier, P. Schlatter, A. Lundbladh, and D. S. Henningson, "Simson: A pseudo-spectral solver for incompressible boundary layer flows," Technical Report KTH, 2007.
[13] J. C. Doyle, "Guaranteed margins for LQG regulators," IEEE Trans. Autom. Control **23**(4), 756–757 (1978).
[14] M. Engert, A. Pätzold, R. Becker, and W. Nitsche, "Active cancellation of Tollmien-Schlichting instabilities in compressible flows using closed-loop control," in *IUTAM Symposium on Flow Control and MEMS* (2008), Vol. 7, pp. 319–331.
[15] E. A. Gillies, "Low-dimensional control of the circular cylinder wake," J. Fluid Mech. **371**, 157–178 (1998).
[16] M. Ilak and C. W. Rowley, "Modeling of transitional channel flow using balanced proper orthogonal decomposition," Phys. Fluids **20**, 034103 (2008).
[17] J.-N. Juang and R. S. Pappa, "An eigensystem realization algorithm for modal parameter identification and model reduction," J. Guid. Control Dyn. **8**(5), 620–627 (1985).
[18] J. Kim, P. Moin, and R. Moser, "Turbulence statistics in fully-developed channel flow at low Reynolds-number," J. Fluid Mech. **177**, 133–166 (1987).
[19] Y. Li and M. Gaster, "Active control of boundary-layer instabilities," J. Fluid Mech. **550**, 185–205 (2006).
[20] N. R. Losse, R. King, M. Zengl, U. Rist, and B. R. Noack, "Control of Tollmien-Schlichting instabilities by finite distributed wall actuation," Theor. Comput. Fluid Dyn. **25**, 167–178 (2011).

[21] Z. Ma, S. Ahuja, and C. W. Rowley, "Reduced order models for control of fluids using the Eigensystem Realization Algorithm," Theor. Comput. Fluid Dyn. **25**(1), 233–247 (2011).
[22] B. C. Moore, "Principal component analysis in linear systems: Controllability, observability, and model reduction," IEEE Trans. Autom. Control **26**(1), 17–32 (1981).
[23] J. Nördstrom, N. Nordin, and D. S. Henningson, "The fringe region technique and the Fourier method used in the direct numerical simulation of spatially evolving viscous flows," SIAM J. Sci. Comput. **20**(4), 1365–1393 (1999).
[24] C. W. Rowley, "Model reduction for fluids using balanced proper orthogonal decomposition," Int. J. Bifurcation Chaos **15**(3), 997–1013 (2005).
[25] O. Semeraro, S. Bagheri, L. Brandt, and D. S. Henningson, "Feedback control of three-dimensional optimal disturbances using reduced-order models," J. Fluid Mech. **677**, 63–102 (2011).
[26] L. Sirovich, "Turbulence and the dynamics of coherent structures, parts I–III," Q. Appl. Math. **3**, 561–590 (1987).
[27] S. Skogestad and I. Postlethwaite, *Multivariable Feedback Control: Analysis and Design*, 2nd ed. (John Wiley and Sons, 2005).
[28] K. Zhou, J. C. Doyle, and K. Glover, *Robust and Optimal Control* (Prentice Hall, 1996).